Estimating the critical temperature of a ferromagnetic material using the 2D Ising model

Bror Hjemgaard, Håkon Kvernmoen, Carl Martin Fevang

November 23, 2020

Abstract

We implemented the Ising model in two dimensions with periodic boundary conditions and no external magnetic field using the Monte Carlo based Metropolis algorithm. We derived the analytical expressions for a 2×2 lattice and found that these corresponded with our numerical implementation. A 2×2 lattice required ca. 10^3 Monte Carlo cycles to reach a state of equilibrium, whilst a 20×20 lattice required around $10^{4.2}$ cycles, implying that the equilibrium time could be lattice size-dependent. Counting the number of times each energy appears we found that higher temperatures gives a higher variance and thus a greater spread in the probability distribution. Optimizing the code and running in parallel with 4 threads made the runtime decrease by a factor of 2.9 ± 0.1 compared with running in series. This speed improvement allowed us to determine the critical temperature to be 2.272 ± 0.007 J/k, compared to the analytical value of 2.269 J/k.

1 Introduction

While the list of physical models of solids is numerous, be it the Einstein solid, the Debye, Fermi or Drude model, few model the phase-transitional behaviour of magnetic solids as accurately as the *Ising Model* does. Due to its simplicity and wide applicability it has become the de facto standard within the superficial studies of magnetic properties. Predicting behaviour like receding magnetization when heated, the Ising model has proven itself invaluable in efforts to further our understanding of magnetic substances. On a technical level, the Ising model is a statistical model of ferromagnetic materials; consisting of atoms in a fixed lattice wherein each atom has a two-state magnetic dipole moment. Allowing each atom to interact with its adjacent neighbours, the Ising model formulates a state of energy dependent on the configuration of each spin. Our study is limited to the two-dimensional lattice with no external magnetic field applied. We will implement periodic boundary conditions, effectively wrapping the lattice around a sphere, creating a continuous grid.

The number of microstates grows exponentially with the lattice size, rendering the calculation of statistical quantities, such as the partition function unfeasible. Therefore we will apply the Metropolis algorithm, a *Markov chain, Monte Carlo* algorithm.

Our goal is to estimate the critical temperature T_C; the point of which a material undergoes a phase transition. Obtaining a realistic and accurate measurement of T_C allows for advanced use and control of magnetic properties within technology, science and medicine. At the heart of almost every modern feat one may find magnetism; be it saving data to the hard drive, operating an MRI machine, listening to the buzzing sound of transformers in an electrical grid or even just pinning your calendar to your magnetic fridge door, one may observe the ever-increasing presence of the magnetic elements around us. We may only further increase this presence by gaining a broader and more thorough understanding of magnetism; which is what we aim to do in this paper by exploring numerical methods for calculating T_C. At the end, you may never look at a refrigerator door the same way again.

2 Theory

2.1 Metropolis algorithm

Our statistical models will exclusively be created using the Metropolis algorithm; a *Markov chain Monte Carlo* algorithm. The term *Markov chain* referring to the fact that the model constructs a sequence of events in which the probability of each event depends on the preceding state. The term *Monte Carlo* broadly refers to the model depending on stochastic, or random, variables. The Metropolis algorithm is effectively a random walk through state space forming a Markov chain of sampled states. A broad, general description of the algorithm is as follows:[1]
Given the probability distribution $\Psi(x)$ of interest, and an arbitrary probability density $\zeta(y)$ with domain $D_{\zeta(y)}$; for a Metropolis calculation of length $N+1$, chose any point of initialization $x_0 \in D_\zeta$, and iterate through $t \in [0, N]$ as follows:

1 Extract a candidate $x' \in D_{\zeta(x_t)}$

2 Calculate a uniformly random number $\alpha \in [0, 1]$

3 if $\alpha \leq \Psi(x')/\Psi(x_t)$, let $x_{t+1} = x'$

4 if $\alpha > \Psi(x')/\Psi(x_t)$, let $x_{t+1} = x_t$

2.2 The 2D Ising Model

We will study the properties and aspects of the 2D *Ising model*. The Ising model is a statistical model of ferromagnetism, based on magnetic dipole moments of atoms in a lattice structure. It models the particles of a material as a crystal lattice-like particle structure in which the energy of each particle is affected by the magnetic dipole moment (spin) of its immediate neighbors. The state of each particle is *binary*, allowing for spin-values of either $+1$ or -1.
For a 2D Ising solid, with no outer magnetic field present, the energy from the spin interactions is given by

$$E = -J \sum_{\langle k,l \rangle}^{N} \varsigma_k \varsigma_l, \tag{1}$$

where N is the number of particles in the lattice, $J > 0$ is an energy coupling and the summation notation $\langle k, l \rangle$ means that we sum over the closest neighbours of each particle only. The values $\varsigma_k = \pm 1$ are the spins of each particle within the lattice.
In the case of $J > 0$, the material at study is labeled "ferromagnetic". Historically, the term "ferromagnetic" has come to classify *any* material that could express spontaneous magnetization, i.e being magnetized without any present external magnetic field. While technically lacking, this term is still in use today.[2]
This spontaneous magnetization is a result of the cumulative magnetic dipole moments of all atoms within the material[3]:

$$M = \sum_{k}^{N} \varsigma_k. \tag{2}$$

Thus, naturally, a ferromagnetic material expresses its greatest spontaneous magnetization when a great majority of the individual atomic spins point in the same direction.
We will assert *periodic boundary conditions* on the lattice; meaning the neighbours of the edging particles are the ones on the *other* side of the lattice, effectively wrapping the lattice around a sphere such that the spectra of particles is continuous.
We will limit our study to the square lattices of size $N = L \times L$, where there are 2^{L^2} possible (unique) spin arrangements of the indistinguishable particles.

2.3 Critical temperature T_C

As T approaches the critical temperature[4] T_C, a phase transition commences.
Near the critical temperature T_C, several physical quantities approach a behaviour modeled through a power law. In the case of an Ising lattice model, the

[1] We will specialize and tweak the implementation of this general method to better fit of our purpose later

[2] P Somasundaran. *Encyclopedia of surface and colloid science*. New York: Taylor & Francis, 2006. ISBN: 9780849396083.

[3] In reality there is a proportionality relation between M and the sum in (2), but the proportionality is irrelevant and we will thus ignore it.

[4] Also sometimes referred to as the "Curie temperature"

mean magnetization, heat capacity and susceptibility are given by

$$\langle M(T)\rangle \sim (T - T_C)^{\beta}, \qquad \beta = \frac{1}{8} \tag{3}$$

$$\chi(T) \sim |T - T_C|^{\gamma}, \qquad \gamma = \frac{7}{4} \tag{4}$$

$$C_V(T) \sim |T - T_C|^{\alpha}, \qquad \alpha \to 0^- \tag{5}$$
$$\sim \ln|T - T_C|$$

The correlation length ξ near T_C goes like

$$\xi(T) \sim |T - T_C|^{-\nu}. \tag{6}$$

As soon will be shown, at high temperatures, $T \gg T_C$, the spins become randomly distributed. At these temperatures it is therefore reasonable to assume ξ to be proportional to the lattice width:

$$\xi = aL = |T - T_C|^{-\nu}$$
$$\Rightarrow T_C(L) = aL^{-1/\nu} + T_C(\infty), \tag{7}$$

where a is some constant of proportionality, and we in the second step applied finite size scaling. Inserting (7) into (3), (4) and (5) yields the new expressions

$$\langle M(T)\rangle \sim L^{-\beta/\nu}, \tag{8}$$

$$C_V(T) \sim L^{\alpha/\nu}, \tag{9}$$

$$\chi(T) \sim L^{\gamma/\nu}. \tag{10}$$

In 1944 the Norwegian-born American physical chemist Lars Onsager obtained the analytical solutions of the 2D Ising model in a zero-field:[5]

$$T_C(\infty) = \frac{2}{\ln\left(1 + \sqrt{2}\right)} \approx 2.269. \tag{11}$$

3 Implementation

The code for the Ising model is written in `C++`. Plotting and data analysis is done in `Python`. All the code for simulations, plotting and timing, as well as how to use it, is openly available at https://github.com/hkve/FYS3150/tree/master/Project4.

[5] Lars Onsager. "Crystal Statistics. I. A Two-Dimensional Model with an Order-Disorder Transition". In: *Phys. Rev.* 65 (3-4 1944), pp. 117–149. URL: https://link.aps.org/doi/10.1103/PhysRev.65.117.

3.1 Adapting the Metropolis algorithm

Several properties of the Ising model allows us to efficiently specialize the implementation of the Metropolis algorithm. First of all, a general trait of the Metropolis algorithm, is that the comparison to the uniformly random number α only depends on the *ratio* $\Psi(x')/\Psi(x_t)$, meaning any probability distribution $P \propto \Psi$ suffices. Thus, we do not need to calculate Z in (19) as it only serves as a constant of proportionality. Thus the ratio becomes

$$\frac{P(s')}{P(s_t)} = \frac{Ze^{-\beta E(s')}}{Ze^{-\beta E(s_t)}}$$
$$= e^{-\beta\Delta E}, \quad \Delta E \equiv E(s') - E(s_t). \tag{12}$$

We will chose $\zeta(s)$ by inferring *single-spin-flip dynamics*; meaning that the proposed system s' is the same as s_t except with *one* atom having its spin flipped. Particularly *which* atom is flipped is uniformly randomly chosen at probability $1/L^2$.[6]
We will refer to one Monte Carlo cycle (MCC) as L^2 random spin-flip proposals. The number of MCCs will be a measurement of the scale of our computations.
Choosing the single-spin-flip method has several advantages, one of them being that at close to equilibrium temperatures the states only differ in energy by small amounts, and another is that by doing single flips one can always get from any one state to another. Furthermore, in flipping only one spin, the change in energy ΔE between the states is only dependent on the value of the flipped spin and its immediate neighbors. Flipping spin ς_l to $-\varsigma_l$ yields the change in energy

$$\Delta E = -J(-\varsigma_l)\sum_{\langle k\rangle}\varsigma_k - (-J\varsigma_l)\sum_{\langle k\rangle}\varsigma_k$$
$$= 2J\varsigma_l\sum_{\langle k\rangle}\varsigma_k. \tag{13}$$

Since $\varsigma_l = \pm 1$ and $\varsigma_k = \pm 1$, there are only 5 possible values $\Delta E = 8J, 4J, 0, -4J, -8J$. Thus in order to

[6] Note that this is only a proportionality change to our previous probability distributions, and thus, by the ratio in the Metropolis algorithm, has no effect on our calculations.

drastically reduce computation time, we will calculate the 5 possible values of $w \equiv e^{-\beta\Delta E}$ pre-iteration and lookup the correct w value when necessary.
The computation at each iteration thus reduces to only computing the sum (13), and we may rephrase our specialized Metropolis implementation as such:
Select an arbitrary initial spin $(L \times L)$ state s_0. For one MCC, iterate over $t \in [0, L \times L - 1]$ accordingly:

1 Propose a new state s' through a spin flip at a randomly picked spin ς_l in s_t

2 Calculate ΔE through (13), and lookup corresponding $w = e^{-\beta\Delta E}$.

3 Generate a uniformly random $\alpha \in [0, 1]$.

4 if $\alpha \leq w$: accept spin flip proposal: $s_{t+1} = s'$.

5 if $\alpha > w$: decline spin flip proposal: $s_{t+1} = s_t$.

Intuitively this method can be understood as such: if $\Delta E \leq 0$ (implying $w \geq 1 \geq \alpha$), we always accept the flip proposal because a lower energy state is always favourable. The comparison of w to α may be described as: "if $\Delta E > 0$ accept the proposal with probability $e^{-\beta\Delta E}$", effectively unfavourably weighing down the higher energy states.

3.2 Periodic boundary conditions

The implementation of periodic boundary conditions only becomes troublesome at the edges of the lattice. We came up with two solutions to this problem; the first of which stores the indices of the neighbor of each particle in array, and another by applying the modulo operator. We will preform a simple time-comparison test between these two implementations and decide which to use considering readability, ease of use and performance.

3.2.1 Index array

This implementation requires constructing an array Λ of length $L + 2$:

$$\Lambda = [L - 1, 0, 1, 2, \ldots, L - 2, L - 1, 0] \,.$$

Letting Λ_i, $i \in [0, L + 1]$, be the i'th element in Λ, the four neighbours of ς_l at index (x, y) are

$$\begin{aligned} \text{Left: } (\Lambda_x, y) \quad & \text{Right: } (\Lambda_{x+2}, y) \\ \text{Above: } (x, \Lambda_y) \quad & \text{Below: } (x, \Lambda_{y+2}) \end{aligned}$$

where $x, y \in [0, L-1]$. The advantage to this method of neighbour-lookup is that it is exactly that; a lookup. No computation is needed. However, the disadvantage is that it quickly becomes confusing having to deal with several indexes at once.

3.2.2 Modulo operator

Another approach is a more generic and mathematical one, using the native `C++` modulo operator. The indices of the four neighbours are thus

$$\begin{aligned} \text{Left: } \big(\mathrm{mod}_{(x-1+L)}(L), y\big) \quad & \text{Right: } \big(\mathrm{mod}_{(x+1+L)}(L), y\big) \\ \text{Above: } \big(x, \mathrm{mod}_{(y-1+L)}(L)\big) \quad & \text{Below: } \big(x, \mathrm{mod}_{(y+1+L)}(L)\big) \end{aligned}$$

where $\mathrm{mod}_a(z)$ defines the modulo of z, base a. This method does require some integer operation and to improve readability, function calls. The latter can be avoided simply by implementing it as a `inline function`.

3.3 Random number generator

It is noteworthy that due to the small changes between states in the single-spin-flip method, the system if very sensitive to biased decisions, and the quality of our results thus heavily depend on the quality of the random number generator (RNG) used. We have opted to use the 64-bit version of the Mersenne Twister generator (`mt19937_64`), and assume that it is sufficient for all our purposes.

3.4 Optimization

Solving the system for large L is computationally expensive and may take a long time to compute. It is therefore of reasonable to suggest attempting to increasing performance through parallelization and vectorization. The loop in the Metropolis algorithm serves as the main bottleneck in our computations, but unfortunately this algorithm contains conditional

statements which cannot be written as mask assignments and optimization through vectorization is unfeasible here. We add a `-O3` compile flag to our code to preform optimizations where possible.
Parallelization on the other hand, allows us to share the workload of our program between multiple threads. As we will be running our later computations for many different temperatures, dividing this workload can presumably increase performance. The two main main options for parallelization in `C++` are `MPI` and `OpenMP`. After trying both methods we used `OpenMP` due to its ease of implementation. `OpenMP` uses a shared memory-mode processors (SMP) model, meaning that all threads will share memory and data.[7] One thread runs from start to finish, initializing and taking inputs. This is called the master thread. The parallel part is the actual simulation such that multiple threads can run multiple simulations simultaneously. These are called the slave threads. When a slave thread is done it merges with the master thread. Unfortunately `OpenMp` is not black magic and does create some overhead when spawning and merging threads. Thus the benefits from parallelization will be more apparent when running for larger lattice sizes or many MCCs.

4 Method

4.1 Benchmarking

We will test the accuracy and dependency of our model by comparing our numerical results to analytical values for a 2×2 lattice. Appendix D derives these formulae, and we will compare the numerical and analytical values of the mean energy $\langle E \rangle$, the mean magnetization $\langle |M| \rangle$, the specific heat capacity C_V and the susceptibility χ as functions of T. This will allow us to discover potential bugs in our implementation, increasing the computational efficiency as well as give us a general idea of the number of MCCs necessary to achieve accurate results.
Thereafter we will build upon the latter; broadening our study to that of the dependency upon the number of MCCs. By this point, we should have encountered the convergence towards the point of equilibrium mentioned above, and we will attempt to estimate the number of MCCs needed to reach the point of equilibrium. It is critical to achieve an accurate estimation of the number of MCCs needed to reach equilibrium as we cannot compute accurate expectation values whilst the state is not in one of its most probable states.

4.2 Estimating T_C

While our approach to estimating the critical temperature will be understandable from the Results-section alone, some elements of the process are still noteworthy. Our aim is to reproduce the value in (11) as accurately as possible by calculating (7) for several L, setting $\nu \to 1$ and doing a linear fit along along L^{-1}. The task is thus reduced to extracting T_C from the computed $\langle E \rangle, \langle |M| \rangle, C_V$ and χ. From the above theory we may describe the behaviour of the different functions as follows:
(3): at $T = T_C$ the function will experience a relatively substantial shift due to the small size of $\beta = 1/8$ (not the same β as in Boltzmann statistics!). The shift is, however, not instantaneous and the function will most likely experience a negative slope around T_C rather than an instant shift.
(4) is symmetric around T_C, where it spikes. The spiking is however not sharp due to $\gamma = 7/4$.
(5) has a sharply defined spike at $T = T_C$ because the expression goes like $\lim_{\alpha \to 0^-} 0^\alpha \to \infty$.
Out of the three, C_V shows the most mathematical potential to stand out at $T = T_C$, hence we will meticulously compute C_V in order to accurately extract T_C to use in (7). In order for C_V to have a definite spike, we must ensure a high resolution in T, as the above limit is only true when T is *very* close to T_C.

[7] Alexandre E. Eichenberger et al. *OMPT: An OpenMP Tools Application Programming Interface for Performance Analysis*. Ed. by Alistair P. Rendell, Barbara M. Chapman, and Matthias S. Müller. Berlin, Heidelberg: Springer Berlin Heidelberg, 2013, pp. 171–185.

L	$t_{idx}[s]$	$\sigma_{idx}[s]$	$t_{mod}[s]$	$\sigma_{mod}[s]$	Imp %
10	0.652	0.002	0.678	0.013	3.863
20	2.917	0.316	3.025	0.644	3.567
30	7.358	0.089	7.543	0.416	2.454
40	13.057	0.083	13.552	0.510	3.654
50	20.463	0.269	21.050	0.171	2.787

Table 1: Comparing the timing of the indexing- and modulo methods when dealing with periodic boundary conditions. We ran tests in the range $L = [10, 50]$ with 10 tests for each L and method. t_{idx} and t_{mod} are the times used by the indexing- and modulo method, respectively. The "Imp" denotes the relative improvement between the method index- and modulo method. All tests were preformed over 10^5 MCCs.

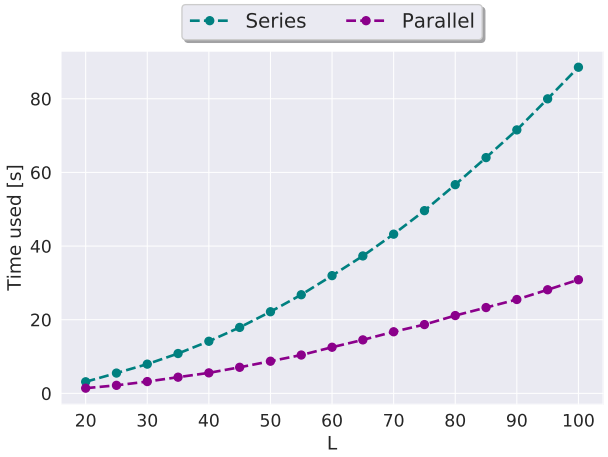

Figure 1: Time comparison for different lattice sizes L. We used 12 different temperatures for each L and plotted the mean time. The parallel runs used 4 threads and gave a speedup of 2.2 ± 0.1 for $L = 20$, 2.5 ± 0.1 for $L = 50$ and 2.9 ± 0.1 for $L = 100$. Each run used 10^5 MCCs.

5 Results

We refer the reader to Appendix B for an explanation of the units used henceforth.

5.1 Periodic boundary condition

When picking the optimal implementation of the periodic boundary conditions, we preformed a timing two proposed methods. The results can be seen in Table 1. As predicted, indexing through Λ outperforms the modulo method, but the improvement is only by about $2\% - 3\%$. Due to this minuscule difference, its readability and ease of use, we opted to use the modulo method.

5.2 Optimizations

In Figure 1 we can see a comparison of mean time spent for multiple lattice sizes, running in both series and in parallel using 4 threads. When running in series the time spent grew rapidly with the lattice size and used on average a little over 80s for a 100×100 lattice. The parallel runs on the other hand performed better for all lattice sizes tested. For a 20×20 lattice it preformed around 2.1 times faster than the computations running in series and for a 100×100 lattice around 2.9 times faster. Clearly the speedup is more significant for bigger lattice sizes. This is due to `openMP` having some overhead, spawning and merging threads. This overhead is less significant when the actual simulations are bigger, since the time used to merge the threads is less significant compared with the simulation time.

5.3 2×2 lattice

Firstly, in order to test the results of our numerical implementation, we studied the 2×2 lattice; a simple system for which the desired values are analytically computable (see Appendix D). Therefore, letting $T = 1$, we used the numerical and analytical expressions of $\langle E \rangle$, $\langle |M| \rangle$, C_V and χ, picked an arbitrary large number of MCCs[8]; and produced the four plots in Figure 2.
The red lines in Figure 2 show the analytical values, clearly tightly overlapping with the produced datapoints in black. Table 2 lists the mean relative error between the analytical and numerical results in Fig-

[8] MCCs $= 10^6$, to be exact

	$\langle E \rangle$	$\langle \lvert M \rvert \rangle$	C_V	χ
$\bar{\epsilon}_{\text{rel}}$	$5.76 \cdot 10^{-4}$	$3.48 \cdot 10^{-4}$	$4.21 \cdot 10^{-3}$	$5.35 \cdot 10^{-3}$

Table 2: Mean relative error between the numerical and analytical values in Figure 2.

ure 2. Having validated our implementation of the Ising model, at least in the case $L = 2$, we proceeded to study the number of necessary MCCs required to achieve an accurate result, as 10^6 MCCs is excessive in most cases. Thus, still for $L = 2$, at $T = 1$ we calculated the four thermodynamical quantities as functions of MCCs, shown in Figure 3.
In Figure 3 the values seem to converge stably to the analytical ones (red line) at $\sim 10^3$ MCCs. Henceforth we will refer to the number of MCCs necessary to reach a stable state as the *equilibrium time* τ.

5.4 20×20 lattice

5.4.1 Approaching equilibrium

We continue or study of τ, this time for $L = 20$. Similarily to the 2×2 case, we graphed the mean energy per particle and magnetization per particle for MCCs ranging from 1 to 10^6, for two temperatures $T = 1$ and $T = 2.4$ and two different initial spin orientations (random or uniform); shown in Figure 4.
Figure 4 illustrates the expected; as the number of MCCs increases, the means converge. At $T = 1$, for both initial spin states, the energy and magnetization converge to $\sim$ -2.0 and $\sim$ 1.0 respectively, while at $T = 2.4$ the energy and magnetization, again independent of initial spin state, converge to $\sim$ -1.2 and ~ 0.45 respectively.
While fluctuating before stabilizing, we may extract an equilibrium time of $\tau \approx 10^{4.2}$ MCCs. The values seem to converge earlier, somewhat below $\tau = 10^3$, similar to the case of $L = 2$. However, the true stability does not kick in before somewhat after 10^4.

During a Monte Carlo cycle, several state changes are proposed, but only some are accepted. A proposed state of lower energy is always favoured, and thus, by the convergent values in Figure 4, we should expect more accepted spin flip proposals for higher T. By counting the number of accepted flips, we produced the graphs in Figure 5.1.
Figure 5.1 confirms our expectations, as more flip proposals are accepted in the higher temperature case. Furthermore, while the low-temperature graphs are noisy, the noise is drastically reduced slightly after 10^4 MCCs, coinciding with τ in Figure 4.
One MCC covers L^2 flip proposals, meaning we may define an acceptance rate R as follows:

$$R \equiv \frac{A}{L^2 M}, \tag{14}$$

where A is the number of accepted flips and M is the number of MCCs. We thus expect $R(T = 1) \ll R(T = 2.4)$ at equilibrium; confirmed by Figure 5.2 which plots R against MCCs. There are barely any state changes in the low temperature case, while the higher temperature confirms over 25% of all proposals.

5.4.2 Probability distribution

Another important aspect is the shape of the probability distribution $P(E)$. In order to study this we created two histograms of the number of different energies in the two cases $T = 1$ (Figure 6.1) and $T = 2.4$ (Figure 6.2).
The bins of the histograms have width $dE = 0.01$, because, according to our previous studies, the only possible values[9] of ΔE are: $\Delta E = \pm 0.01, \pm 0.02, 0$.
Some noteworthy results, that later will be discussed, is that no state of energy $E = -1.99$ occurs for $T = 1$ and that there are more possible energy states when $T = 2.4$, where the distribution is normal.

5.5 The critical temperature T_C

Finally we aim to estimate T_C. (7) requires we calculate $T_C(L)$ for *at least* 2 different, preferably large, L. We therefore study the four cases of $L = 40, 60, 80, 100$. Our approach is as such: calculate the thermodynamical quantities over a large T domain, similar to Figure 2, in order to estimate

[9] adjusted into units of J per total number of spins

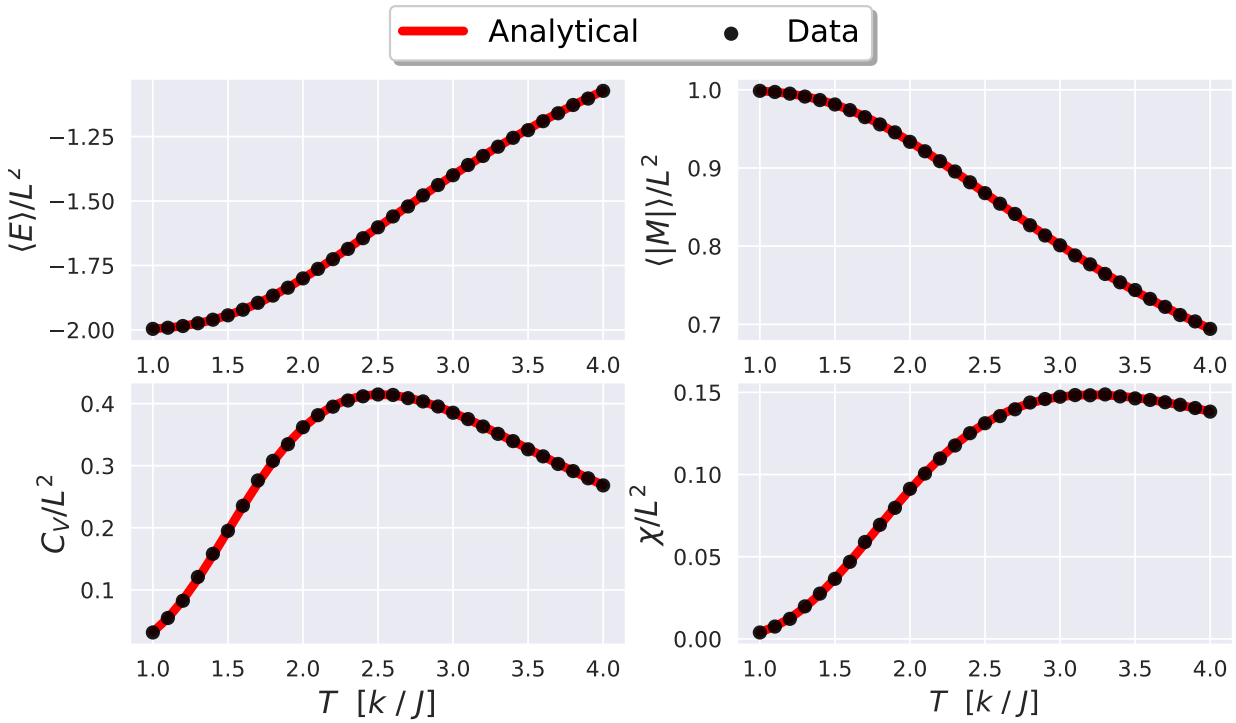

Figure 2: 2.1 (upper left): $\langle E \rangle$, 2.2 (upper right): $\langle |M| \rangle$, 2.3 (bottom left): C_V, 2.4 (bottom right): χ. Analytical values (red line) compared to computed values (black dots), computed with 10^6 MCCs and $dT = 0.1$, for a 2×2 lattice.

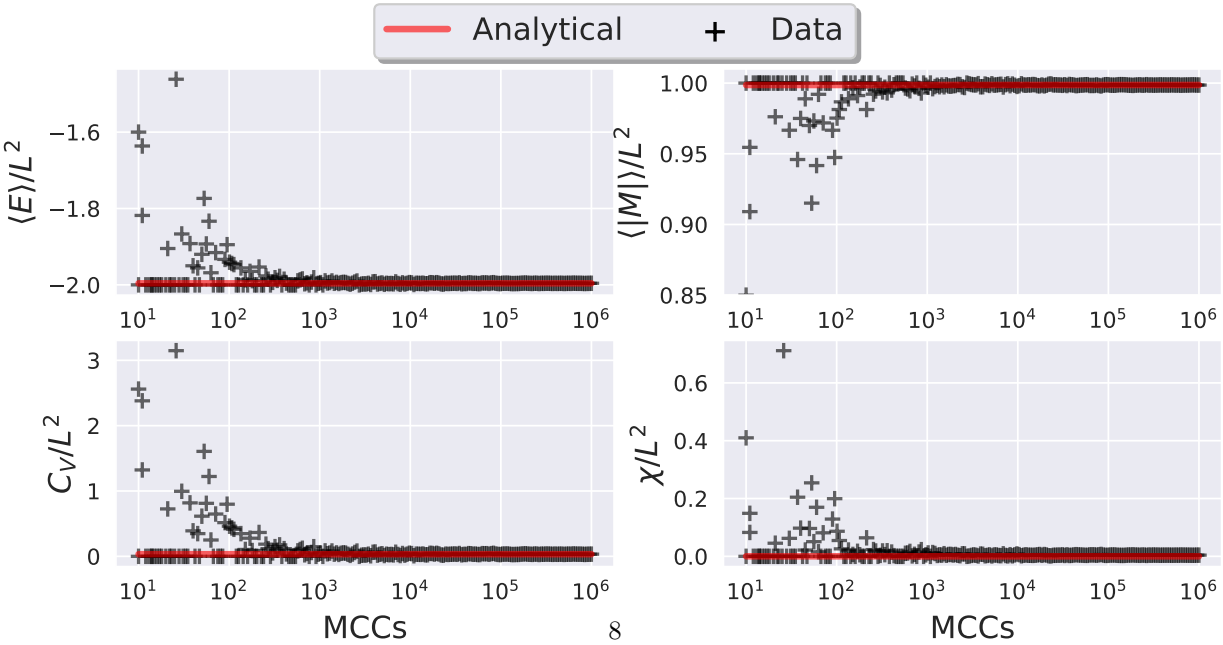

Figure 3: 3.1 (upper left): $\langle E \rangle$, 3.2 (upper right): $\langle |M| \rangle$, 3.3 (bottom left): C_V, 3.4 (bottom right): χ. Analytical values (red line) compared to computed values (black marks), computed for MCCs ranging from 10 to 10^6 for a 2×2 lattice with $T = 1$.

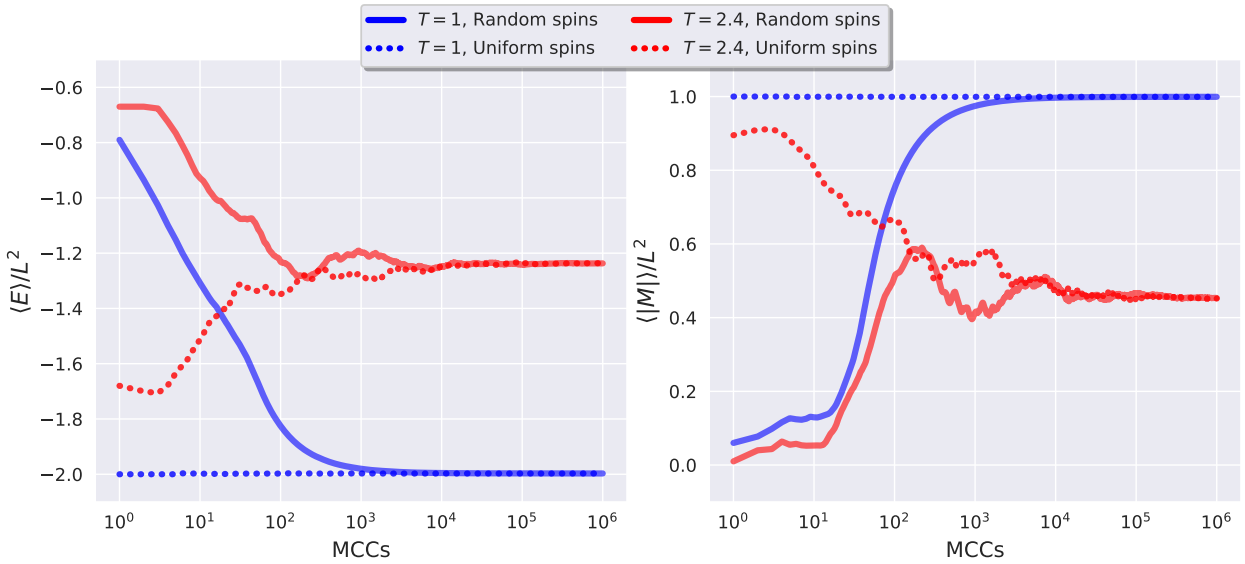

Figure 4: 4.1 (left): Mean energy, 4.2 (right): magnetization per particle. Both in a 20×20 lattice for MCCs ranging from 1 to 10^6 for temperatures $T = 1, 2.4$ as well as for different initial spin states (solid = random initial spins, dashed = uniform initial spins)

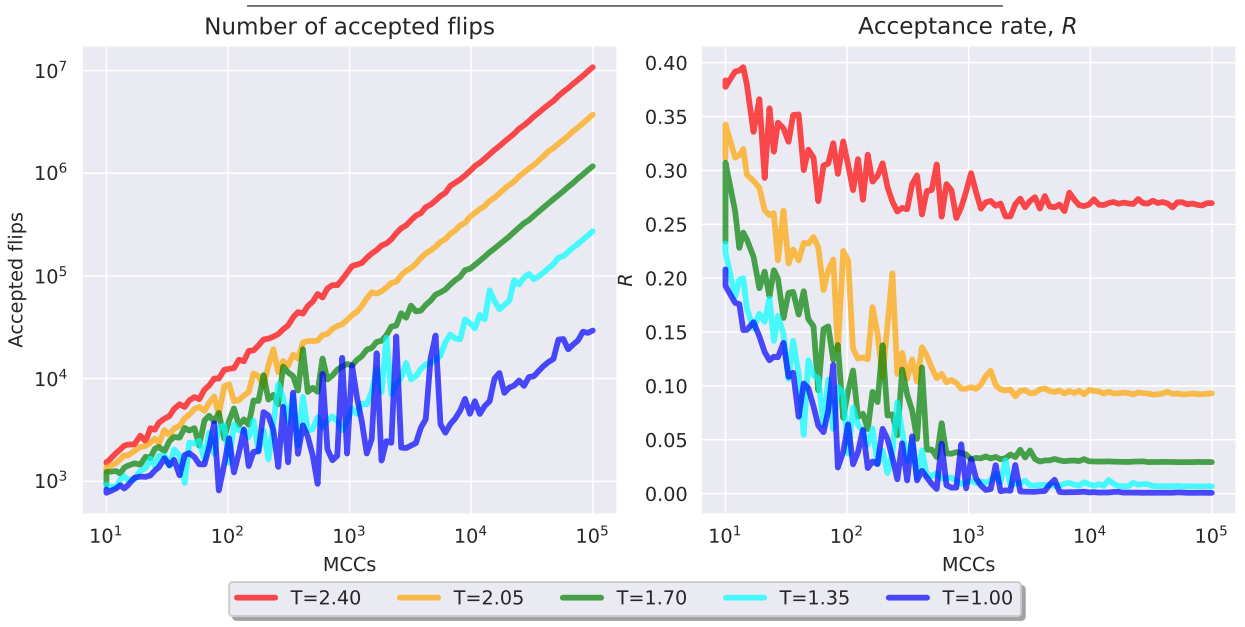

Figure 5: 5.1 (left): Number of accepted flip proposals as a function of MCCs for a 20×20 lattice at different temperatures. 5.2 (right): The acceptance rate R for 4 different temperatures.

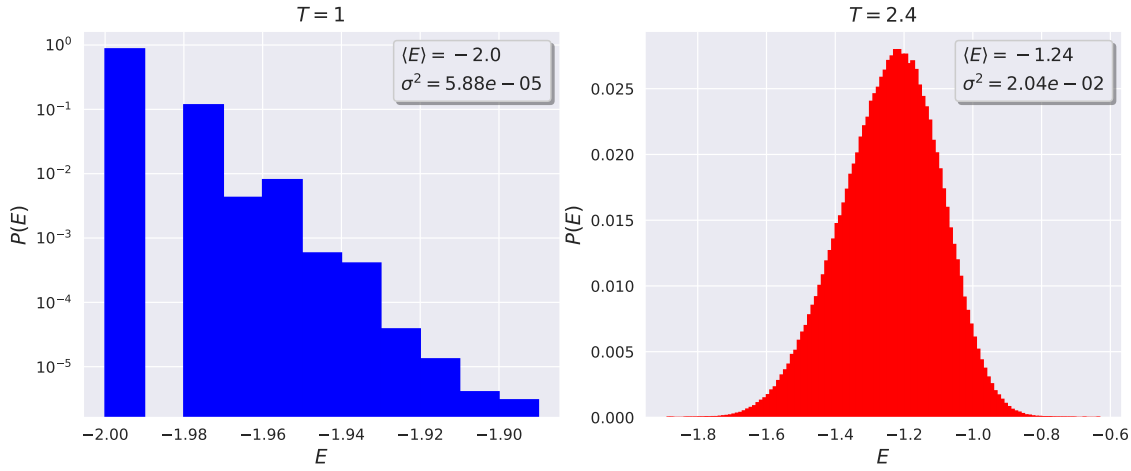

Figure 6: Figure 6.1 (left): Probability $P(E)$ for $T = 1$, Figure 6.2 (right): Probability $P(E)$ for $T = 2.4$. Both in a 20×20 lattice for MCCs $= 10^6$. Please note that the y-axis in Figure 6.1 is logarithmic. Energy in units J/L^2.

a smaller domain wherein we suspect $T_C(L)$ to lie. Thereafter increase the resolution in T and use more MCCs to re-calculate the thermodynamical quantities in this narrow domain in order to extract $T_C(L)$.
We ran a simulation over the domain $T \in [2, 2.5]$ with $dT = 0.01$, $\tau = 10^{4.2}$ and 10^5 MCCs. As this simulation was mostly qualitative, we opted to not plot every datapoint but rather a fitted curve with the `UnivariateSpline`-method of `scipy.interpolate` in `python`, shown in Figure 7.

The observed shapes of Figure 7 are as predicted in the Method-section, which we shall go into further detail about later. Nevertheless, all 4 graphs experienced shifts around $T \in [2.25, 2.30]$, and, also as expected, the heat capacity C_V had the most sharp and definite behaviour here. We therefore opted to calculate C_V through a higher resolution simulation with $dT = 0.001$ and 10^6 MCCs, yielding Figure 8.1. Again, using the `UnivariateSpline`-method, smooth curves were fitted to the data points in order to extract T at the peak of the curves, listed in Table 3. Each $T_C(L)$ has an intrinsic uncertainty of ± 0.001 due to the resolution of the calculation.

L	T_C [J/k]
40	2.287754
60	2.283048
80	2.281198
100	2.277788

Table 3: The extracted critical temperatures T_C from Figure 8.1 for different L

Applying linear regression to these 4 values yielded Figure 8.2 and, by (7), ultimately resulted in a critical temperature of

$$T_C = 2.272 \pm 0.007 \text{ J/k}. \tag{15}$$

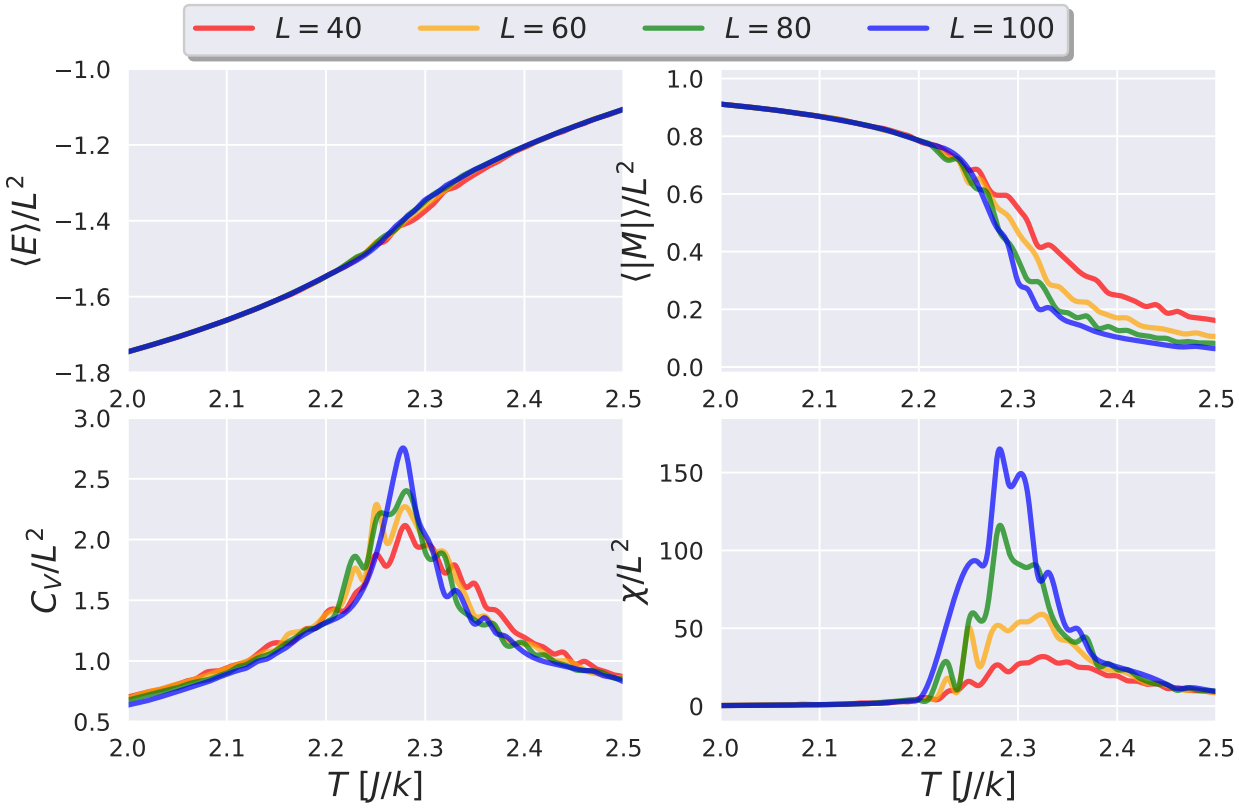

Figure 7: 7.1 (upper left): $\langle E \rangle$, 7.2 (upper right): $\langle |M| \rangle$, 7.3 (bottom left): C_V, 7.4 (bottom right): χ. All as functions of T for $dT = 0.01$, MCCs $= 10^5$, $\tau = 10^{4.2}$.

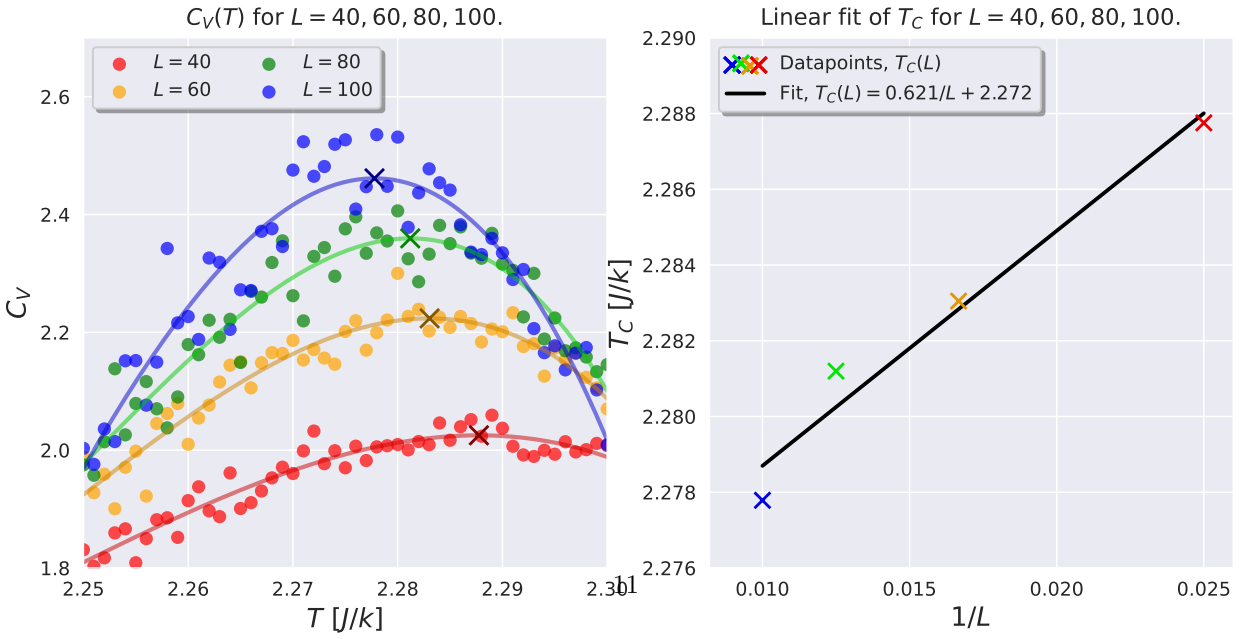

Figure 8: 8.1 (left): Heat capacity C_V (per spin) computed for $dT = 0.001$, 10^6 MCCs, $\tau = 10^{4.2}$, as well as fitted curves to estimate the extrema. 8.2 (right): The extrema in Figure 8.1 used to calculate T_C.

6 Discussion

Consider two states, s and s', with opposite spins, meaning $\varsigma_k = -\varsigma'_k$. The magnetization of the states are thus of course opposite; $M = -M'$, but they have equal energy:

$$E' = -J \sum_{\langle k,l \rangle} \varsigma'_k \varsigma'_l = -J \sum_{\langle k,l \rangle} (-\varsigma_k)(-\varsigma_l)$$
$$= -J \sum_{\langle k,l \rangle} \varsigma_k \varsigma_l = E.$$

By Boltzmann statistics, the two states must therefore be equally probable. This means that the systems spends on average as much time in the state s with magnetization M as in s' with magnetization $M' = -M$. Therefore the average magnetization over a long period of time should be zero.

Furthermore we may describe the mean absolute value of the magnetization as a measure of the ratio between the number of different spins; $|M| = 0$ implying there are an equal amount of spin up/down and $|M| = 1$ implying the spins are all up or down. Clearly these two mean values will often be close to one another (especially at high T), and we may take this as the argument as to why we are allowed to substitute $\langle M \rangle \to \langle |M| \rangle$ in (25).

This qualitatively explains the statistical reason as to why the convergent value of $\langle |M| \rangle$ in Figure 4 is lower for $T = 2.4$ than $T = 1$. Furthermore this coincides with the magnetization in Figure 7, as it approaches 0 for large T. We may visualize this claim by simply drawing the individual spins of each atom for high and low T. This process is shown in Figure 9 for a 500×500 system with a random initial state through 200 MCCs.

Figure 9.2 depicts what we already knew; at high temperatures the state is effectively random and the drawn spin state looks like TV-static. A more interesting remark comes from Figure 9.1, wherein the spins have congealed into groups of identical spins. The reasoning behind this lies in the fact that the system is only 200 MCCs deep into the computation, and the congealed groups are merely an indication of the uniform spin distribution that is to follow as the number of MCCs increases. We may conclude as follows: for low temperatures the binding energies of (1) favours systems in which neighbouring particles have identical spins. Therefore a low-temperature system chooses to have a few large surface areas of similar spins, minimizing the total number of opposite-spin neighbours, whilst a high-temperature system is impervious to the relative state between neighbours and therefore defaults into a system of unpredictability and randomness.

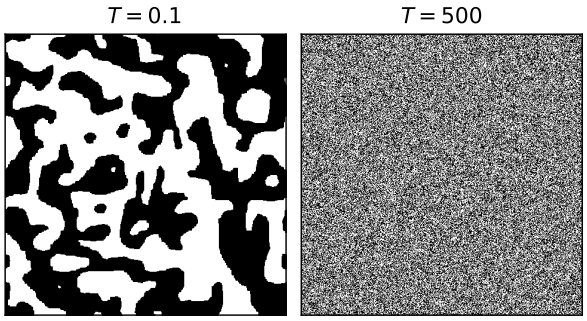

Figure 9: 9.1 (left): Spin orientations for $T = 0.1$. 9.2 (right): Spin orientations for $T = 500$. Both cases for a 500×500 system after 200 MCCs. White/black pixels correspond to spin up/down, respectively.

From our results as well as from the theory of the Ising model, we know that as the phase transitions commences, the energy and magnetization suddenly shift. Ideally this sudden change should resemble a *unit step function*. Therefore, by their definition through differentiation of E and M, we expect C_V and χ to resemble a *dirac-δ* function[10] centered on T_C, suddenly spiking at $T = T_C$. This coincides with the results in Figure 7 as well as the predictions in the Method-section.

6.1 2×2 lattice

Not only acting as an effective benchmark, Figure 2 also illustrates several expected and interesting elements. Firstly, the mean energy $\langle E \rangle$ gradually increases with T, which fits our prediction of ther-

[10] Ronald Newbold Bracewell. *The Fourier transform and its applications (3rd ed.)* New York, NY: McGraw-Hill., 2000. ISBN: 0-07-303938-1.

mal energy eventually overwhelming the neighbor-spin energies and pushing the model to a system of random spin-orientation and thus lower neighbour-spin-energy. Also, at $T = 1$, the energy is -2, the lowest possible value, further confirming that the spin distribution is uniform at low temperatures.
Secondly, the mean absolute magnetization $\langle|M|\rangle$, follows an opposite path to that of $\langle E\rangle$, decreasing from a maximum value of $\langle|M|\rangle = 1$ at $T = 1$ towards $\langle|M|\rangle = 0$ as T increases. Again, this coincides with our predictions and the results of $\langle E\rangle$: when the spin distribution is uniform, the mean absolute magnetization simply equals the number of spin-particles. All the values in Figure 2 are "per-spin", and thus $\langle|M|\rangle = 1$ at $T = 1$ is exactly as expected. As temperature increases, disorder ensues and at a state of total randomness (very high T), one should have $\langle|M|\rangle = 0$; which seems to be the direction Figure 2.2 seems to be headed.

6.2 20×20 lattice

6.2.1 Equilibrium time, τ

Studying Figure 4, the convergent value is clearly independent of initial spin state, as is expected. It is, however, noteworthy that in the case of ordered initial spin with $T = 1$, the energy and magnetization stays constant over all MCCs. This may be explained as follows: at low temperature the energy is at its minimum, meaning the spins have little reason to change its state (no lower energy state exists). There are some minor fluctuations due to chance, but on average they are canceled out. Since the energy stays constant, the state s, and therefore the magnetization, does too. This is the reason as to why $\langle E\rangle$ and $\langle|M|\rangle$ have the same equilibrium time τ.
It is both reasonable and realistic to suggest that the equilibrium time depends on L, and in order to ensure the most accurate results from the other sections of this paper we should have implemented a more dynamical system and method for evaluating τ in order to ensure both efficient and accurate computation.

6.2.2 Probability distribution

The results of Figure 6 effectively illustrates several elements of the Ising model. Firstly, studying Figure 6.1 and keeping in mind that the y-axis is logarithmic, we observe that the probability of the state being in the uniform spin-state (lowest energy) is undoubtedly largest. Thereafter a steady (logarithmic) decline follows.
The bins of the histograms are of width 0.01, which begs the question as to why there are no measured states with energy -1.99, as it, seemingly, is only one change of $\Delta E = +0.01$ away from the most likely state. The reason is easily determined from (13): When the system is in its uniform state with $E = -2$ and a new state is proposed, the flipped spin will always have spin opposite to *all* its neighbours, yielding a necessary change in energy of $+8J \to \Delta E = +0.02$. This reasoning also holds in the reverse process, leaving states of energy -1.99 impossible.
At $T = 1$, the system therefore favours a state of uniform spin; because any change of state therefrom would require the largest change in energy possible ($+8J$) which is physically unfavourable. Furthermore, this also explains why the probabilities for $T = 1$ seem to occur pairwise (neighbouring bins seem to be of approximately similar height); because the chance of two events of prob. e^{-4} happening successively is as probable as one event of prob. e^{-8} happening.
Lastly, moving our attention to Figure 6.2 for $T = 2.4$, a normal distribution is formed. The mean is $\langle E\rangle = -1.24$, which nicely coincides with the convergent values in Figure 4.1. Here too the bins are of size 0.01, although as no state is as extremely favoured as in the case of $T = 1$, the distribution is more evenly spread.
The above discussions and conclusions may also be seen from the variances listed in Figure 6, where $\sigma_E^2(T = 1) < \sigma_E^2(T = 2.4)$. By statistical theory this effectively tells us that the energies are more spread out in the higher temperature case.
From the above studies it is reasonable to conclude that the (stable) mean energy increases with T. This conclusion sounds rather obvious; as it is natural to claim that the energy within a system increases with

temperature. However, this claim if often based in the empirical, and we have arrived at this conclusion based on statistical data and simulations.

6.3 The critical temperature T_C

Our result of $T_C = 2.272 \pm 0.007$ J/k is extremely close to the analytical value (11), deviating only by 0.12%. It is however very likely that our estimated error of ± 0.007 is too small, as it only reflects the standard deviation obtained through the linear regression and does not account for the aforementioned resolution of $dT = 0.001$. In order to further decrease this error one may either decrease dT or increase the number of MCCs. This increased accuracy could also yield a χ-graph from which T_C was definitely ascertainable.
Increasing the number of MCCs will make the fitted curves smoother and more accurate as the data will be less spread along the y-axis. Implementing the above mentioned dynamic τ system could both decrease computation time and increase accuracy. Lastly, by further decreasing dT the resolution required to accurately depict the peak of χ may be obtained, allowing us to estimate T_C through both C_V and χ. Nevertheless, we are satisfied with our estimation.

7 Concluding remarks

By implementing the 2D Ising-model through the Metropolis algorithm we obtained a computed critical temperature of a ferromagnetic material without the presence of an external field of $T_C = 2.272 \pm 0.007$ J/k, only 0.12% away from the analytical value. We successfully modeled and predicted several known aspects and properties of a ferromagnetic substance undergoing phase transition, and gained invaluable insight into the fundamental construction and applicability of numerical models of materials.
Even though we achieved a very accurate estimation of T_C, we have also listed several ways as to how this estimation may be improved upon as efficiently as possible. The most efficient way of improving the results would be to implement a dynamical τ system which takes into account the lattice size L.
Furthermore this proved as great practice of implementing vectorization and parallelization and the general importance of code optimization in the case of the computationally demanding.
Lastly, and most importantly, we gained great insight into the very core and essence of ferromagnetism; into the engine which drives the numerous technologies surrounding us, from kitchen appliances to the Large Hadron Collider, at the core they are all controlled by the "spinning" charges of particles.

Quantity	E	M	T	β	C_V	χ
Unit	J	–	Jk^{-1}	J^{-1}	k	J^{-1}

Table 4: The standardized units used in this report.

8 Appendix

A Statistical theory

The *expected value/mean*, $\langle A \rangle$, of a random variable A picked from a discrete probability distribution $P : \{a_1, a_2 \dots a_N\} \to \{p_1, p_2 \dots p_N\}$ is given by

$$\langle A \rangle = \sum_{i=1}^{N} p_i a_i. \tag{16}$$

The *variance* of A is defined by

$$\sigma_A^2 = \sum_{i=1}^{N} p_i a_i^2 - \left(\sum_{i=1}^{N} p_i a_i \right)^2 \tag{17}$$

$$= \left\langle A^2 \right\rangle - \langle A \rangle^2. \tag{18}$$

Its square root, σ_A, is called the *standard deviation*.

B Units

In all our calculations and simulations we use natural units of J and k. We do this because we want to work with quantities with a order of magnitude 1, which avoids underflow and overflow. The specific units of each of the thermodynamic quantities are presented in Table 4. Furthermore, unless explicitly noted otherwise, *all* our computed quantities are per particle. This drastically simplifies the comparisons between computations of different lattice sizes.

C Boltzmann statistics and thermodynamics

The probability $P(s)$ of finding a system in a state s with energy $E(s)$ is given through Boltzmann statistics as

$$P(s) = \frac{1}{Z} e^{-\beta E(s)}, \tag{19}$$

where the *partition function* Z for N particles in a $L \times L$ Ising model-lattice, is given by

$$Z(T) = \sum_{s} e^{-\beta E(s)}, \tag{20}$$

where the sum is over each possible microstate s with energy $E(s)$ and $\beta = 1/kT$ is the Boltzman factor. For a system at temperature T, the expectation value of A with value $A(s)$ in the state s is given by

$$\langle A \rangle = \frac{1}{Z} \sum_{s} A(s) e^{-\beta E(s)}. \tag{21}$$

The mean energy $\langle E \rangle$ may also be found analytically through

$$\langle E \rangle = -\frac{1}{Z} \frac{\partial Z}{\partial \beta} = -\frac{\partial \ln Z}{\partial \beta} \tag{22}$$

and is related to the heat capacity at constant volume C_V through:

$$C_V = \frac{\partial \langle E \rangle}{\partial T} = -\frac{\beta}{T} \frac{\partial \langle E \rangle}{\partial \beta} = \frac{\beta}{T} \frac{\partial^2 \ln(Z)}{\partial \beta^2}$$

$$= \frac{\beta}{T} \left(\left\langle E^2 \right\rangle - \langle E \rangle^2 \right) = \frac{\beta}{T} \sigma_E^2. \tag{23}$$

Furthermore, the average magnetization M of a system of N particles is given by

$$\langle M \rangle = \frac{1}{N} \sum_{k}^{N} \varsigma_k, \tag{24}$$

and the magnetic susceptibility χ is related to M by its variance. To get smoother results for the susceptibility around the critical temperature, we use the absolute value of the magnetization[11]. Thus the susceptibility is given by:

$$\chi = \beta \left(\left\langle M^2 \right\rangle - \langle |M| \rangle^2 \right) = \beta \sigma_M^2. \tag{25}$$

[11] For more information see (Robert Strawderman. "Monte Carlo Methods in Statistical Physics by M. E. J. Newman; G. T. Barkema". In: *Journal of the American Statistical Association* 96 [Jan. 2001]. DOI: 10.2307/2670314)

State	$\begin{matrix}\uparrow\uparrow\\ \uparrow\uparrow\end{matrix}$	$\begin{matrix}\uparrow\downarrow\\ \downarrow\uparrow\end{matrix}$	$\begin{matrix}\uparrow\uparrow\\ \uparrow\downarrow\end{matrix}$	$\begin{matrix}\downarrow\downarrow\\ \downarrow\downarrow\end{matrix}$
E [J]	-8	8	0	-8
M [-]	4	0	2	-4

Table 5: Four possible states for a 2×2 Ising model along with their corresponding energy and magnetization

$\uparrow$ / $\downarrow$	E [J]	M [-]	deg.
4 / 0	-8	4	1
3 / 1	0	2	4
2 / 2	0	0	4
2 / 2	8	0	2
1 / 3	0	-2	4
0 / 4	-8	-4	1

Table 6: All possible energies, E, and magnetizations, M, for a 2×2 Ising model lattice. The first column counts the number of up-/down-spins in the state. The degeneracies add up to 16 different states.

D Analytical study: 2×2 lattice

Out of the 16 possible states ($2^{2^2} = 16$) some examples of possible states and their corresponding energies and magnetizations are listed in Table 5. Due to both rotational and translational symmetry inferred by the periodic boundary conditions, the energies are degenerate. Rather than individually listing them, we have counted the energy and magnetization for each possible orientation and listed them by degeneracy in Table 6.

Inserting the values from Table 6 into the thermodynamical equations of Appendix C we get the analytical expressions for a 2×2 Ising lattice:

$$\begin{aligned} Z(T) &= 12e^{0} + 2e^{8\beta J} + 2e^{-8\beta J} \\ &= 12 + 4\cosh(8\beta J)\,. \end{aligned} \tag{26}$$

$$\begin{aligned} \langle E\rangle &= \frac{1}{Z}\left(-8Je^{8\beta J} + 2\cdot 8Je^{-8\beta J} - 8Je^{8\beta J}\right) \\ &= \frac{-32J}{Z}\sinh(8\beta J) \\ \langle E^2\rangle &= \frac{1}{Z}\left((-8J)^2e^{8\beta J} + 2\cdot(8J)^2e^{-8\beta J} + (-8J)^2e^{8\beta J}\right) \\ &= \frac{256J^2}{Z}\cosh(8\beta J) \\ \langle |M|\rangle &= \frac{1}{Z}\left(4e^{8\beta J} + 4\cdot 2e^{0} + 4\cdot|-2|e^{0} + |-4|e^{8\beta J}\right) \\ &= \frac{8}{Z}\left(2 + e^{8\beta J}\right) \\ \langle M^2\rangle &= \frac{1}{Z}\left(4^2e^{8\beta J} + 4\cdot 2^2e^{0} + 4\cdot(-2)^2e^{0} + (-4)^2e^{8\beta J}\right) \\ &= \frac{32}{Z}\left(1 + e^{8\beta J}\right) \end{aligned}$$

Finally, by (23) and (25) we get

$$\begin{aligned} C_V &= \frac{1024\beta J^2}{TZ^2}\left(3\cosh(8\beta J) + 1\right), \\ \chi &= \frac{32\beta}{Z}\left(1 + e^{8\beta J}\right) - \frac{64\beta}{Z^2}\left(2 + e^{8\beta J}\right)^2. \end{aligned}$$

References

Onsager, Lars. "Crystal Statistics. I. A Two-Dimensional Model with an Order-Disorder Transition". In: *Phys. Rev.* 65 (3-4 1944), pp. 117–149. URL: https://link.aps.org/doi/10.1103/PhysRev.65.117.

Palstra, T.T.M. et al. "Study of the critical behaviour of the magnetization and electrical resistivity in cubic La(Fe, Si)13 compounds". In: *Journal of Magnetism and Magnetic Materials* 36.3 (1983), pp. 290 –296.

Bracewell, Ronald Newbold. *The Fourier transform and its applications (3rd ed.)* New York, NY: McGraw-Hill., 2000. ISBN: 0-07-303938-1.

Strawderman, Robert. "Monte Carlo Methods in Statistical Physics by M. E. J. Newman; G. T. Barkema". In: *Journal of the American Statistical Association* 96 (Jan. 2001). DOI: 10.2307/2670314.

Somasundaran, P. *Encyclopedia of surface and colloid science*. New York: Taylor & Francis, 2006. ISBN: 9780849396083.

Eichenberger, Alexandre E. et al. *OMPT: An OpenMP Tools Application Programming Interface for Performance Analysis*. Ed. by Alistair P. Rendell, Barbara M. Chapman, and Matthias S. Müller. Berlin, Heidelberg: Springer Berlin Heidelberg, 2013, pp. 171–185.